Mon. Not. R. Astron. Soc. **390,** 733–740 (2008) doi:10.1111/j.1365-2966.2008.13768.x

Reference ultraviolet wavelengths of Cr III measured by Fourier transform spectrometry

D. G. Smillie,[1] J. C. Pickering[1]★ and P. L. Smith[2]

[1]*Blackett Laboratory, Imperial College London, London SW7 2BZ*
[2]*Harvard–Smithsonian Center for Astrophysics, 60 Garden Street, Cambridge, MA 02138, USA*

Accepted 2008 July 29. Received 2008 July 1

ABSTRACT

We report Cr III ultraviolet (UV) transition wavelengths measured using a high-resolution Fourier transform spectrometer (FTS), for the first time, available for use as wavelength standards. The doubly ionized iron group element spectra dominate the observed opacity of hot B stars in the UV, and improved, accurate, wavelengths are required for the analysis of astronomical spectra. The spectrum was excited using a chromium–neon Penning discharge lamp and measured with the Imperial College vacuum ultraviolet FTS. 140 classified $3d^3 4s$–$3d^3 4p$ Cr III transition lines, in the spectral range 38 000 to 49 000 cm^{-1} (2632 to 2041 Å), the strongest having wavelength uncertainties less than one part in 10^7, are presented.

Key words: atomic data – line: identification – methods: laboratory.

1 INTRODUCTION

The iron group elements, with their complex spectra and relatively high abundances, provide much of the observed opacity in stellar atmospheres (Johansson 1987). In particular, doubly ionized spectra of the iron group are observed to dominate the ultraviolet (UV) spectra of hot B stars (Swings, Klutz & Vreux 1976; Cowley & Frey 1988). Major improvements in the resolution and accuracy of observed stellar spectra in the past few decades, made possible by advances in space and ground-based spectrographs, have led to a demand for transition wavelengths in the vacuum ultraviolet (VUV) wavelength region with uncertainties as low as a few parts in 10^7 (approximately 0.2 mÅ at 2000 Å) in order to fully interpret newly resolved stellar spectral features (Leckrone et al. 1996; Smith et al. 1998). The existing atomic data base of laboratory measurements for the doubly ionized iron group spectra has been found to be severely lacking in wavelength coverage and accuracy, with order of magnitude improvements in wavelength accuracy required in many cases (Pickering 2002). For complex spectra, laboratory measurements are essential because theoretically calculated wavelengths and energy levels are of insufficient accuracy for many astrophysical applications (Kurucz 2002).

Fourier transform (FT) spectroscopy enables highly accurate, high resolution, broad-band spectral measurements, and has been used in the recent years to measure neutral and singly ionized iron group spectra yielding improved wavelengths and energy levels; see, for example: Cr I (Murray 1992); Fe I (Nave et al. 1994); Co I (Pickering & Thorne 1996) and Co II (Pickering et al. 1998). Doubly ionized iron group spectra, in particular Cr III, Fe III and Co III, have also been studied using FT spectroscopy with a Penning discharge lamp (PDL) as a light source (Smillie et al., in preparation; Smith et al. 1998; Smillie et al. 2006). This paper presents accurate wavelengths of Cr III measured by FT spectroscopy for use as wavelength standards and for analysis of stellar spectra.

The most recent analysis of a doubly ionized iron group element is that of Ekberg (1997), an improvement and extension of his analysis of Cr III from Ekberg (1976). Ekberg used a low-voltage sliding spark discharge and the normal incidence vacuum spectrograph at the US National Institute of Standards and Technology (NIST) to measure Cr III in the region 763 to 2675 Å. In total, Ekberg presents 1893 transition lines and 352 energy levels with typical level uncertainties ranging from 0.05 to 0.15 cm^{-1}. The observed wavelengths are quoted with estimated uncertainties of 5 mÅ. Ekberg's observed wavelength uncertainties correspond to two parts in 10^6 at 45 000 cm^{-1}, an order of magnitude greater uncertainty than required for analysis of high-resolution stellar spectra. In the new measurements of Cr III transition lines by FT spectroscopy, presented here, the wavenumber (σ) uncertainty approaches 0.002 cm^{-1} (0.1 mÅ at 2200 Å, or five parts in 10^8) for the lines of high signal-to-noise ratio (SNR), more than an order of magnitude improvement in accuracy over Ekberg's measurements.

Fig. 1 shows a section of the observed and synthetic spectra of the B star γ Pegasus (Adelman, Peters & Proffitt, private communication), recorded by the Space Telescope Imaging Spectrograph (STIS) onboard the *Hubble Space Telescope* (*HST*). Of the 43 identified lines labelled in Fig. 1, 40 are from the doubly ionized iron group spectra; 14 are Cr III lines, 11 of which are included in our classified Fourier transform spectrometer (FTS) linelist.

2 EXPERIMENTAL DETAILS

The Cr III spectrum was acquired in the wavenumber range 31 596 to 63 192 cm^{-1}, using the Imperial College (IC) VUV FTS, described

★E-mail: j.pickering@imperial.ac.uk

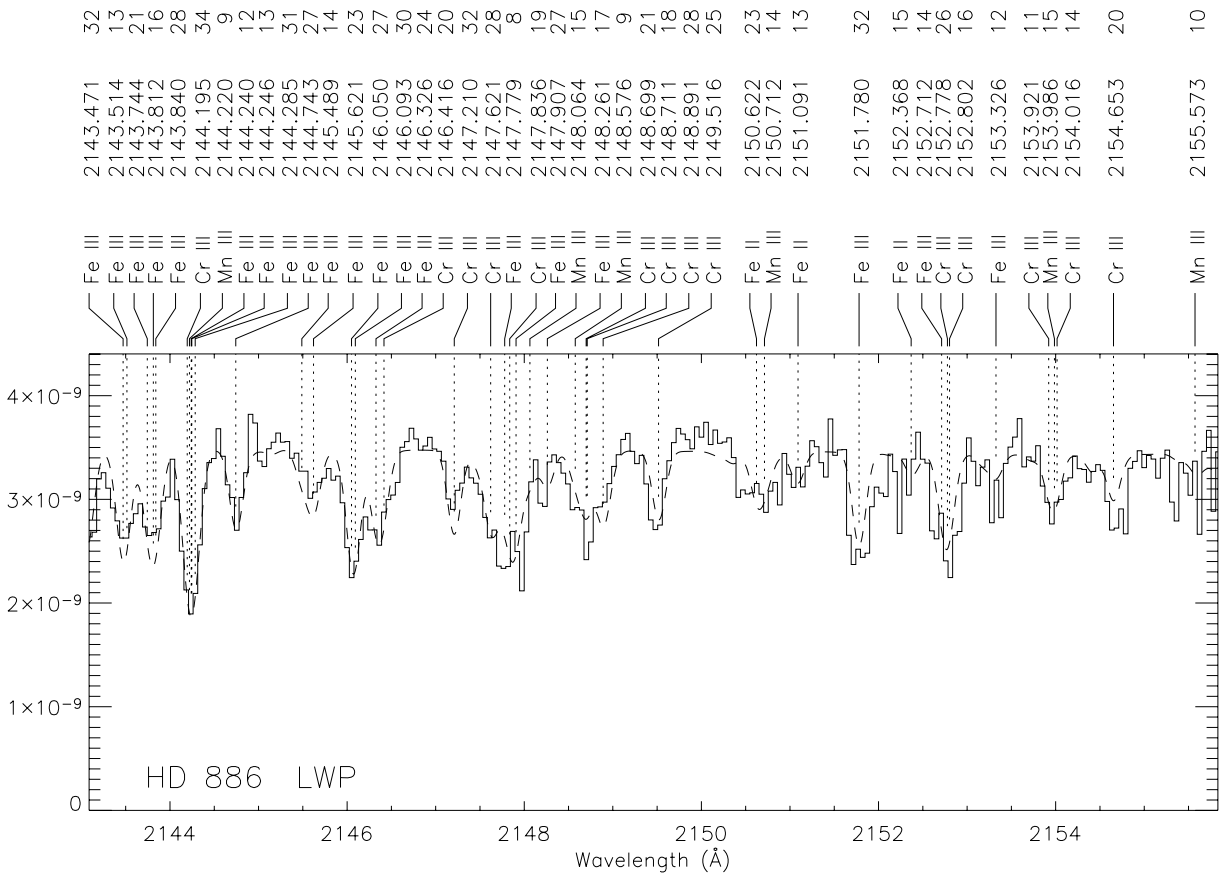

Figure 1. A section of the *HST*/STIS spectrum of the B star γ Pegasus with identified lines labelled. The solid and dashed lines are the observed and synthetic spectra, respectively (Adelman, private communication).

by Thorne (1996), and a PDL as light source. The spectral resolution used, 0.12 cm^{-1}, was sufficient to fully resolve the Doppler broadened transition line profiles, for which the average unblended full-width at half maximum (FWHM) was just under 0.3 cm^{-1}.

Emission-line sources used for exciting neutral and singly ionized iron group spectra for measurements with an FTS, such as the hollow cathode lamp, are unable to significantly excite the levels of the doubly ionized iron group elements. However, a PDL designed by Heise et al. (1994) has been shown to populate the levels of certain doubly ionized iron group elements while maintaining the necessary intensity stability for measurements by FTS (Smith et al. 1998). For the Cr III measurements, the PDL was operated with pure (99.9 per cent) chromium cathodes, a neon buffer gas of pressure 3.0 to 4.4 $\times$ 10^{-4} mBar and a DC discharge current of 1.9 A; the discharge voltage was in the range 0.93 to 1.14 kV (Smillie 2007). The success in running the PDL using Cr cathodes is contrary to the predictions of Finley et al. (1979), who studying a similar PDL, predicted that chromium cathodes would be unsatisfactory due to their magnetic properties. Excitation of the doubly ionized levels in the PDL is optimized by using a higher discharge current and a lower buffer gas pressure; however, instability in the discharge increases as the conditions become more extreme, imposing a practical limit on the lamp operating conditions. Thus, the singly ionized state remains the dominant one, and in the case of chromium, a bandpass filter (peak transmission wavelength at 2200 Å, FWHM approximately 200 Å) was required to suppress strong Cr II transition lines. (Strong lines contribute noise to the interferogram and thus to all regions of the spectrum; the resulting noise level in the spectrum can mask weak Cr III lines.) A Hamamatsu R7154 photomultiplier tube was used as a detector. Lines in the Cr III $3d^3 4s$–$3d^3 4p$ transition array were observed with 144 scans co-added to improve the SNR in the spectrum. A portion of the chromium–neon (Cr–Ne) PDL spectrum, showing the classified Cr III lines, is presented in Fig. 2.

3 WAVELENGTH AND INTENSITY CALIBRATION

The recorded Cr III spectrum was analysed, using the XGREMLIN program (Nave, Sansonetti & Griesmann 1997), to yield a linelist with line wavenumbers, SNR, FWHM and relative intensities. A Voigt profile was fitted to the spectral features using a least-squares method. The wavenumber uncertainty, $\Delta\sigma$, is given by (Davis, Abrams & Brault 2001)

$$\Delta\sigma = \frac{\mathrm{FWHM}}{\mathrm{SNR}\sqrt{n}}, \tag{1}$$

where n is the number of data points across the line FWHM (typically five to six points with the resolution used in this work). In a few cases, poor line fits using a Voigt profile led to some lines being fitted using a centre-of-gravity (COG) line fit. The COG-fitting uncertainty is proportional to $\frac{\mathrm{FWHM}}{\mathrm{SNR}}$, although it may be greater for weaker lines due to the difficulty in distinguishing between the noise and the edge limits of the line profile.

After fitting of the spectral lines, wavenumber calibration was carried out by comparison with a set of wavelength standard lines (Learner & Thorne 1988), giving a wavenumber dependent

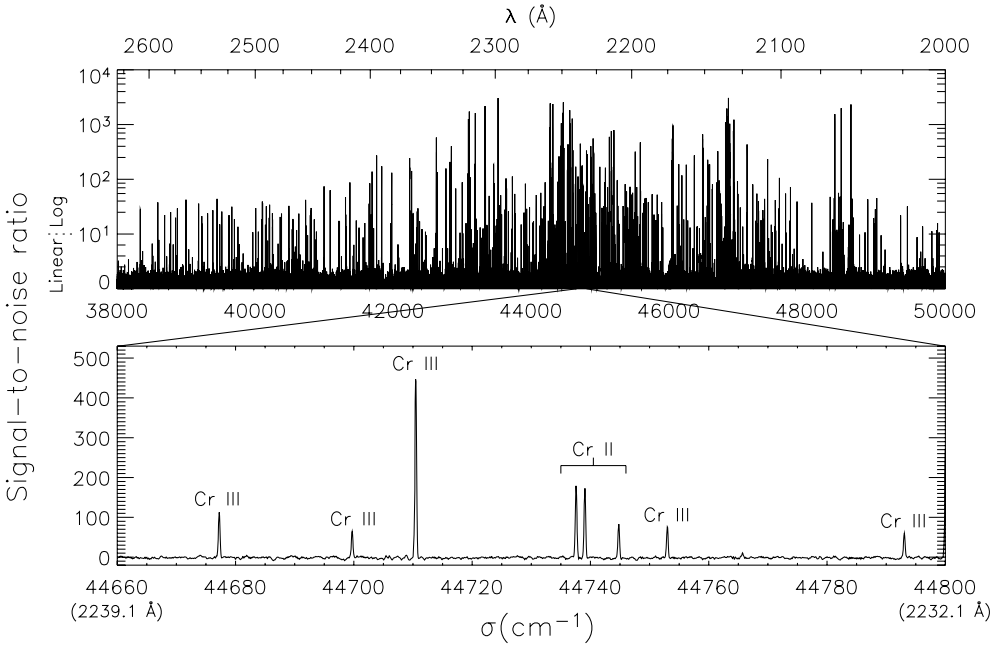

Figure 2. A portion of the Cr–Ne PDL spectrum recorded by the IC VUV FTS, incorporating all of the classified Cr III lines, with a small 7 Å section expanded. Note that the $0 \leq \mathrm{SNR} \leq 10$ portion of the upper figure is linear.

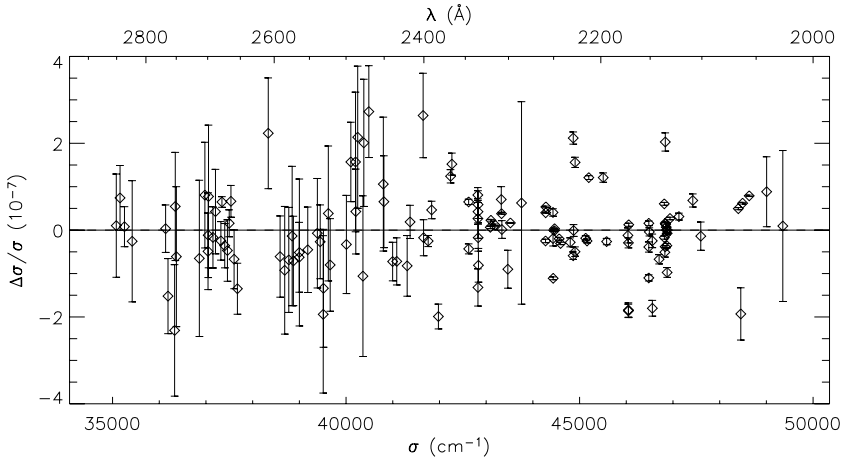

Figure 3. Comparison between standard spectral line wavenumbers and the equivalent lines observed in the Cr–Ne PDL spectrum after wavenumber calibration. The error bars represent the line-fitting uncertainties of the new measurements alone.

shift:

$$\sigma_{\mathrm{true}} = (1 + k)\sigma_{\mathrm{meas}}, \tag{2}$$

where k is a constant. The standard lines for the wavelength calibration were taken from a spectrum comprising Cr I, Cr II and Ne gas lines, recorded by FTS (Murray 1992). This chromium HCL spectrum was recently recalibrated (Pickering, private communication), giving Cr I and Cr II wavenumbers relative to the Ar II standards of Whaling et al. (1995) with the wavenumber uncertainty of 0.002 cm^{-1} in the UV. Fig. 3 shows the comparison between these standard lines and those from our Cr–Ne PDL spectrum after wavenumber calibration, where the uncertainties in the plot are the line-fitting uncertainties of the PDL lines. Combining the standard error from Fig. 3 with the wavenumber uncertainty of the standard lines gives a combined wavenumber uncertainty of just over 0.002 cm^{-1}, or significantly less than one part in 10^7, for the wavenumber calibration. The uncertainty for the strongest lines approaches the wavenumber uncertainty of the wavelength standards.

An intensity-calibrated deuterium standard lamp was used to find the instrument response. Fig. 4 shows the normalized response of the IC VUV FTS for the Cr–Ne PDL measurements, with the experimental setup as described. After intensity calibration, the resulting relative line intensities for strong lines (SNR ≈100) are accurate to within approximately 12 per cent at 44 600 cm^{-1}, falling to approximately 15 per cent at 42 760 and 47 420 cm^{-1}.

4 THE CR III SPECTRAL LINELIST

The classified Cr III lines are presented in Table 1. The first column gives the logarithm of the calibrated integrated line intensities. The

Table 1. The classified Cr III transition linelist observed by FTS.

Integrated intensity[a]	FWHM[b] (cm^{-1})	SNR[c]	λ_{air} (Å)	λ_{vac} (Å)	σ (cm^{-1})	Differences[d] (cm^{-1})	Uncertainty[e] (cm^{-1})	Transition Lower	–	Upper	Note[f]
4.59	0.129	3	2616.5249	2617.3059	38 207.226	−0.114	0.022	$(^2H)4s\,^3H_5$	–	$(^2G)4p\,^3H_5$	
4.65	0.205	3	2587.4101	2588.1842	38 637.127	0.107	0.034	$(^2H)4s\,^3H_6$	–	$(^2G)4p\,^3H_6$	
4.77	0.269	6	2483.0738	2483.8235	40 260.510	−0.020	0.023	$(^4F)4s\,^3F_4$	–	$(^4F)4p\,^3D_3$	
4.71	0.258	4	2479.8177	2480.5666	40 313.370	0.000	0.032	$(^4F)4s\,^3F_3$	–	$(^4F)4p\,^3D_2$	
4.53	0.287	3	2476.5364	2477.2846	40 366.780	−0.001	0.048	$(^4F)4s\,^3F_3$	–	$(^4F)4p\,^5F_4$	
4.23	0.152	5	2413.6469	2414.3806	41 418.490	−0.150	0.015	$(a^2D)4s\,^3D_1$	–	$(^2G)4p\,^3F_2$	II
4.53	0.290	5	2402.9589	2403.6902	41 602.700	0.190	0.029	$(a^2D)4s\,^1D_2$	–	$(a^2D)4p\,^3F_2$	
3.83	0.256	5	2342.4592	2343.1769	42 677.102	−0.028	0.026	$(^4F)4s\,^3F_4$	–	$(^4F)4p\,^3G_4$	
3.77	0.233	8	2340.4890	2341.2063	42 713.024	−0.086	0.015	$(^2G)4s\,^1G_4$	–	$(^2G)4p\,^3F_4$	
4.79	0.287	91	2324.8944	2325.6082	42 999.504	−0.046	0.003	$(^4F)4s\,^3F_4$	–	$(^4F)4p\,^3G_5$	
4.73	0.299	85	2319.0776	2319.7901	43 107.349	−0.071	0.004	$(^4F)4s\,^3F_3$	–	$(^4F)4p\,^3G_4$	G
4.52	0.257	66	2314.6269	2315.3384	43 190.231	0.011	0.003	$(^4F)4s\,^3F_2$	–	$(^4F)4p\,^3G_3$	
3.65	0.317	8	2310.0436	2310.7541	43 275.915	0.025	0.020	$(a^2D)4s\,^3D_2$	–	$(^2P)4p\,^3P_2$	III
3.65	0.317	8	2310.0436	2310.7541	43 275.915	−0.085	0.020	$(a^2D)4s\,^3D_3$	–	$(^2P)4p\,^3P_2$	III
3.49	0.225	8	2308.2767	2308.9868	43 309.040	−0.060	0.014	$(^2G)4s\,^3G_5$	–	$(^2G)4p\,^3H_4$	
3.53	0.255	7	2302.7810	2303.4899	43 412.388	−0.132	0.018	$(^2P)4s\,^3P_0$	–	$(^2P)4p\,^3P_1$	
4.02	0.318	21	2300.5102	2301.2186	43 455.237	0.007	0.008	$(^2G)4s\,^1G_4$	–	$(^2G)4p\,^1G_4$	
3.34	0.225	6	2299.5123	2300.2204	43 474.094	−0.136	0.019	$(^4P)4s\,^3P_2$	–	$(^2P)4p\,^1D_2$	
4.00	0.295	19	2297.9186	2298.6264	43 504.242	−0.028	0.008	$(^2G)4s\,^3G_4$	–	$(^2G)4p\,^3H_4$	
3.53	0.226	10	2297.3116	2298.0193	43 515.735	−0.175	0.011	$(^2P)4s\,^3P_1$	–	$(^2P)4p\,^3P_0$	II
3.97	0.237	27	2295.5628	2296.2701	43 548.884	−0.006	0.005	$(^2H)4s\,^1H_5$	–	$(^2H)4p\,^1G_4$	
3.08	0.174	5	2295.3111	2296.0183	43 553.659	−0.181	0.018	$(^2P)4s\,^3P_1$	–	$(^2P)4p\,^3P_1$	
4.44	0.293	69	2290.6755	2291.3818	43 641.789	−0.011	0.003	$(^2G)4s\,^3G_3$	–	$(^2G)4p\,^3H_4$	
4.03	0.291	27	2289.2555	2289.9615	43 668.857	0.057	0.006	$(^2G)4s\,^1G_4$	–	$(^2G)4p\,^1F_3$	
3.28	0.208	7	2287.1859	2287.8914	43 708.368	−0.132	0.015	$(^2P)4s\,^3P_2$	–	$(^2P)4p\,^3P_1$	
3.86	0.363	13	2286.5909	2287.2962	43 719.742	0.002	0.014	$(^2G)4s\,^3G_5$	–	$(^2G)4p\,^3H_5$	
4.33	0.304	55	2284.4785	2285.1834	43 760.165	0.055	0.003	$(^2G)4s\,^1G_4$	–	$(^2G)4p\,^1H_5$	
2.79	0.116	4	2282.3792	2283.0836	43 800.410	−0.149	0.015	$(^2H)4s\,^3H_6$	–	$(^2H)4p\,^3H_5$	
2.90	0.302	2	2280.6218	2281.3259	43 834.158	−0.182	0.076	$(^2H)4s\,^3H_5$	–	$(^2H)4p\,^3H_4$	
4.01	0.333	25	2277.4797	2278.1831	43 894.628	0.058	0.007	$(^2H)4s\,^3H_4$	–	$(^2H)4p\,^3H_4$	
4.49	0.306	84	2276.4250	2277.1281	43 914.964	0.054	0.003	$(^2G)4s\,^3G_4$	–	$(^2G)4p\,^3H_5$	
4.01	0.297	29	2275.4799	2276.1828	43 933.202	−0.098	0.005	$(^2H)4s\,^3H_5$	–	$(^2H)4p\,^3H_5$	
3.32	0.246	5	2275.2787	2275.9816	43 937.087	−0.073	0.025	$(^4F)4s\,^5F_3$	–	$(^4F)4p\,^5G_2$	
4.03	0.285	32	2273.3510	2274.0535	43 974.339	0.169	0.005	$(^2H)4s\,^3H_6$	–	$(^2H)4p\,^3H_6$	
4.30	0.316	56	2264.9240	2265.6247	44 137.937	0.007	0.006	$(^4F)4s\,^5F_2$	–	$(^4F)4p\,^5G_2$	G
4.51	0.316	89	2261.6945	2262.3945	44 200.957	0.107	0.003	$(^4F)4s\,^5F_3$	–	$(^4F)4p\,^5G_3$	III
4.51	0.316	89	2261.6945	2262.3945	44 200.957	−0.034	0.003	$(a^2D)4s\,^3D_1$	–	$(^2P)4p\,^3D_2$	III
3.08	0.173	6	2258.6224	2259.3217	44 261.072	0.192	0.015	$(^2H)4s\,^1H_5$	–	$(^2H)4p\,^1H_5$	
4.83	0.298	209	2257.9836	2258.6828	44 273.592	−0.018	0.002	$(^4F)4s\,^5F_1$	–	$(^4F)4p\,^5G_2$	
4.62	0.309	110	2257.5586	2258.2577	44 281.926	−0.234	0.002	$(^2G)4s\,^3G_5$	–	$(^2G)4p\,^3H_6$	
4.46	0.307	85	2257.4099	2258.1090	44 284.843	−0.057	0.004	$(^4F)4s\,^5F_4$	–	$(^4F)4p\,^5G_4$	G
3.69	0.247	18	2253.2992	2253.9973	44 365.625	−0.126	0.007	$(^2F)4s\,^3F_3$	–	$(^2F)4p\,^3F_4$	II
4.30	0.308	60	2251.9815	2252.6794	44 391.582	0.042	0.006	$(^4F)4s\,^5F_5$	–	$(^4F)4p\,^5G_5$	G
4.94	0.311	263	2251.4666	2252.1643	44 401.734	0.114	0.002	$(^4F)4s\,^5F_2$	–	$(^4F)4p\,^5G_3$	G
3.05	0.205	5	2251.0319	2251.7295	44 410.307	0.147	0.021	$(^2F)4s\,^3F_4$	–	$(^2F)4p\,^3F_3$	
3.43	0.175	14	2247.6852	2248.3822	44 476.424	0.114	0.007	$(^2F)4s\,^3F_4$	–	$(^2F)4p\,^3F_4$	
5.08	0.311	364	2244.1188	2244.8149	44 547.102	−0.038	0.002	$(^4F)4s\,^5F_3$	–	$(^4F)4p\,^5G_4$	
2.80	0.143	4	2242.8956	2243.5915	44 571.393	−0.197	0.018	$(b^2D)4s\,^3D_1$	–	$(b^2D)4p\,^3D_2$	
4.58	0.315	113	2237.5813	2238.2761	44 677.242	0.052	0.002	$(^4F)4s\,^3F_4$	–	$(^4F)4p\,^3F_4$	
4.33	0.309	65	2236.4562	2237.1508	44 699.714	−0.226	0.003	$(a^2D)4s\,^1D_2$	–	$(a^2D)4p\,^3P_1$	II
5.19	0.313	457	2235.9182	2236.6127	44 710.468	−0.072	0.002	$(^4F)4s\,^5F_4$	–	$(^4F)4p\,^5G_5$	
4.40	0.299	78	2233.7930	2234.4869	44 753.003	−0.037	0.003	$(^4F)4s\,^3F_3$	–	$(^4F)4p\,^3F_3$	
4.31	0.315	61	2231.7951	2232.4886	44 793.062	0.132	0.003	$(^4F)4s\,^3F_2$	–	$(^4F)4p\,^3F_2$	
2.82	0.175	3	2228.7520	2229.4449	44 854.214	0.094	0.029	$(b^2D)4s\,^3D_3$	–	$(b^2D)4p\,^3D_3$	
5.29	0.316	564	2226.6875	2227.3800	44 895.797	−0.173	0.002	$(^4F)4s\,^5F_5$	–	$(^4F)4p\,^5G_6$	
4.02	0.400	24	2224.7426	2225.4346	44 935.043	0.203	0.009	$(^4P)4s\,^3P_1$	–	$(^2P)4p\,^3D_1$	II
3.62	0.263	14	2219.5893	2220.2802	45 039.359	−0.111	0.010	$(^4P)4s\,^5P_3$	–	$(^4P)4p\,^5P_2$	
3.42	0.213	11	2218.7005	2219.3913	45 057.399	−0.061	0.010	$(a^2D)4s\,^1D_2$	–	$(a^2D)4p\,^1F_3$	
3.70	0.285	16	2217.7552	2218.4458	45 076.603	−0.037	0.009	$(^4P)4s\,^5P_2$	–	$(^4P)4p\,^5P_1$	
4.00	0.293	31	2217.5242	2218.2147	45 081.299	−0.161	0.010	$(^2H)4s\,^1H_5$	–	$(^2H)4p\,^1I_6$	G
2.87	0.158	4	2216.2323	2216.9226	45 107.575	0.095	0.020	$(^4F)4s\,^3F_3$	–	$(^4F)4p\,^3F_4$	

Table 1 – *continued*

Integrated intensity[a]	FWHM[b] (cm^{-1})	SNR[c]	λ_{air} (Å)	λ_{vac} (Å)	σ (cm^{-1})	Differences[d] (cm^{-1})	Uncertainty[e] (cm^{-1})	Transition Lower – Upper	Note[f]
3.58	0.380	7	2215.8552	2216.5454	45 115.250	0.010	0.027	$(^2P)4s\,^3P_0$ – $(^2P)4p\,^3D_1$	
3.23	0.263	6	2215.2243	2215.9143	45 128.098	−0.012	0.022	$(a^2D)4s\,^3D_2$ – $(^2P)4p\,^3S_1$	
3.37	0.271	8	2211.4480	2212.1373	45 205.151	−0.049	0.017	$(^4P)4s\,^5P_1$ – $(^4P)4p\,^5P_1$	
3.72	0.502	9	2211.2293	2211.9185	45 209.622	0.112	0.028	$(a^2D)4s\,^3D_2$ – $(^4P)4p\,^3D_3$	III
3.72	0.502	9	2211.2293	2211.9185	45 209.622	0.002	0.028	$(a^2D)4s\,^3D_3$ – $(^4P)4p\,^3D_3$	III
3.80	0.292	19	2208.7063	2209.3950	45 261.259	−0.031	0.008	$(^4P)4s\,^3P_2$ – $(^2P)4p\,^3D_3$	
2.89	0.237	3	2207.4487	2208.1371	45 287.043	−0.127	0.040	$(^4P)4s\,^5P_2$ – $(^4P)4p\,^5P_2$	
2.79	0.160	3	2203.7467	2204.4343	45 363.112	−0.058	0.027	$(^2P)4s\,^3P_2$ – $(^2P)4p\,^3D_3$	
4.14	0.338	35	2203.2312	2203.9187	45 373.724	−0.056	0.005	$(^4P)4s\,^5P_3$ – $(^4P)4p\,^5P_3$	
4.02	0.289	31	2202.0473	2202.7345	45 398.117	0.157	0.005	$(^2H)4s\,^1H_5$ – $(^2H)4p\,^3G_4$	
3.57	0.289	11	2201.9457	2202.6329	45 400.212	−0.128	0.013	$(^4P)4s\,^3P_1$ – $(^2P)4p\,^3D_2$	
3.26	0.358	4	2201.4618	2202.1489	45 410.189	−0.061	0.045	$(a^2D)4s\,^3D_1$ – $(a^2D)4p\,^3F_2$	
3.73	0.358	13	2201.1997	2201.8868	45 415.596	−0.134	0.014	$(^4P)4s\,^5P_1$ – $(^4P)4p\,^5P_2$	
3.25	0.220	5	2201.0190	2201.7061	45 419.323	−0.247	0.022	$(^2G)4s\,^3G_5$ – $(^2G)4p\,^3G_4$	
3.55	0.274	11	2199.0982	2199.7848	45 458.992	0.131	0.013	$(a^2D)4s\,^3D_2$ – $(^4P)4p\,^3D_2$	III
3.55	0.274	11	2199.0982	2199.7848	45 458.992	0.021	0.013	$(a^2D)4s\,^3D_3$ – $(^4P)4p\,^3D_2$	III
4.35	0.316	57	2198.6367	2199.3232	45 468.533	−0.048	0.003	$(^2H)4s\,^3H_4$ – $(^2H)4p\,^3I_5$	
3.88	0.337	19	2197.8976	2198.5840	45 483.820	0.200	0.009	$(^2G)4s\,^3G_3$ – $(^2G)4p\,^3G_3$	
3.00	0.166	5	2194.6529	2195.3387	45 551.059	0.108	0.017	$(^4P)4s\,^5P_3$ – $(^4P)4p\,^3P_2$	
4.04	0.361	25	2191.5896	2192.2747	45 614.722	−0.018	0.007	$(^2G)4s\,^3G_4$ – $(^2G)4p\,^3G_4$	
3.53	0.263	10	2191.2661	2191.9511	45 621.456	−0.024	0.026	$(^4P)4s\,^5P_2$ – $(^4P)4p\,^5P_3$	G
4.08	0.311	32	2190.7723	2191.4572	45 631.738	−0.052	0.005	$(^2G)4s\,^3G_5$ – $(^2G)4p\,^3G_5$	
3.09	0.224	4	2187.9442	2188.6285	45 690.714	0.104	0.028	$(^4P)4s\,^5P_2$ – $(^4P)4p\,^5D_1$	
4.33	0.308	54	2185.0424	2185.7262	45 751.386	−0.025	0.003	$(^2H)4s\,^3H_5$ – $(^2H)4p\,^3I_6$	
3.25	0.200	5	2184.9959	2185.6796	45 752.359	0.089	0.020	$(^2G)4s\,^3G_3$ – $(^2G)4p\,^3G_4$	
4.04	0.336	22	2183.7539	2184.4374	45 778.378	−0.002	0.008	$(a^2D)4s\,^3D_3$ – $(a^2D)4p\,^3F_4$	
3.71	0.317	13	2182.7874	2183.4707	45 798.645	−0.005	0.012	$(^4P)4s\,^5P_2$ – $(^4P)4p\,^3P_2$	
3.71	0.340	9	2181.8077	2182.4907	45 819.210	0.040	0.019	$(^4P)4s\,^5P_1$ – $(^4P)4p\,^5D_1$	
5.18	0.344	320	2171.0571	2171.7380	46 046.071	0.221	0.002	$(^2P)4s\,^3P_1$ – $(^2D)4p\,^3F_2$	II
4.31	0.281	53	2170.7034	2171.3842	46 053.573	−0.247	0.003	$(^2H)4s\,^3H_6$ – $(^2H)4p\,^3I_7$	
3.83	0.328	14	2166.2753	2166.9551	46 147.702	−0.058	0.012	$(^2G)4s\,^3G_5$ – $(^2G)4p\,^3F_4$	
3.82	0.334	13	2159.1081	2159.7865	46 300.873	0.043	0.013	$(^4P)4s\,^5P_3$ – $(^4P)4p\,^5D_3$	
3.55	0.323	7	2157.2071	2157.8851	46 341.670	−0.040	0.023	$(^2P)4s\,^3P_2$ – $(^4P)4p\,^3D_3$	
3.41	0.327	4	2157.1457	2157.8237	46 342.990	0.060	0.041	$(^2G)4s\,^3G_4$ – $(^2G)4p\,^3F_4$	
3.80	0.288	14	2154.6510	2155.3285	46 396.640	−0.030	0.010	$(^4P)4s\,^5P_2$ – $(^4P)4p\,^5D_2$	III
3.80	0.288	14	2154.6510	2155.3285	46 396.640	0.230	0.010	$(^4P)4s\,^5P_2$ – $(^4P)4p\,^3P_1$	III
3.23	0.223	5	2153.9191	2154.5964	46 412.405	−0.105	0.022	$(^4P)4s\,^5P_1$ – $(^4P)4p\,^3P_0$	
2.96	0.156	4	2152.8001	2153.4772	46 436.526	0.126	0.020	$(^2P)4s\,^3P_1$ – $(^4P)4p\,^3D_2$	
3.85	0.347	13	2152.7734	2153.4505	46 437.102	−0.008	0.013	$(^2G)4s\,^3G_4$ – $(^2G)4p\,^3F_3$	
3.63	0.264	10	2149.5157	2150.1921	46 507.472	0.032	0.013	$(^2G)4s\,^3G_3$ – $(^2G)4p\,^3F_2$	
4.07	0.354	20	2148.8843	2149.5606	46 521.136	0.056	0.009	$(^4F)4s\,^5F_2$ – $(^4F)4p\,^5F_1$	
4.06	0.400	17	2148.7022	2149.3785	46 525.078	0.108	0.012	$(^4P)4s\,^5P_1$ – $(^4P)4p\,^3P_1$	III
4.06	0.400	17	2148.7022	2149.3785	46 525.078	−0.152	0.012	$(^4P)4s\,^5P_1$ – $(^4P)4p\,^5D_2$	III
3.01	0.210	3	2147.8332	2148.5093	46 543.898	0.198	0.035	$(^2F)4s\,^3F_2$ – $(^2F)4p\,^3G_3$	
4.22	0.284	34	2147.6172	2148.2932	46 548.580	0.050	0.005	$(^4P)4s\,^5P_2$ – $(^4P)4p\,^5D_3$	
4.36	0.310	43	2147.2138	2147.8898	46 557.324	0.074	0.004	$(^4F)4s\,^5F_3$ – $(^4F)4p\,^5F_2$	
4.56	0.300	68	2144.1944	2144.8698	46 622.877	0.007	0.003	$(^4F)4s\,^5F_4$ – $(^4F)4p\,^5D_3$	
4.73	0.331	88	2141.1884	2141.8631	46 688.324	0.014	0.003	$(^4F)4s\,^5F_5$ – $(^4F)4p\,^5D_4$	
4.55	0.330	56	2139.1366	2139.8109	46 733.101	−0.079	0.004	$(^4P)4s\,^5P_3$ – $(^4P)4p\,^5D_4$	
3.27	0.225	4	2137.9907	2138.6649	46 758.144	0.124	0.056	$(^4F)4s\,^5F_2$ – $(^4F)4p\,^5F_2$	G
3.44	0.279	5	2136.9362	2137.6100	46 781.217	0.067	0.028	$(^2F)4s\,^3F_3$ – $(^2F)4p\,^3G_4$	
4.03	0.274	19	2134.1665	2134.8398	46 841.922	0.042	0.007	$(a^2D)4s\,^3D_2$ – $(a^2D)4p\,^3D_1$	
4.99	0.323	146	2133.8077	2134.4810	46 849.797	−0.003	0.002	$(^4P)4s\,^3P_0$ – $(^2P)4p\,^3S_1$	II
3.28	0.191	5	2129.5878	2130.2602	46 942.622	0.052	0.019	$(b^2D)4s\,^3D_1$ – $(b^2D)4p\,^3F_2$	
3.63	0.349	5	2126.5015	2127.1733	47 010.745	0.105	0.035	$(b^2D)4s\,^3D_2$ – $(b^2D)4p\,^3F_2$	
3.65	0.273	7	2123.5569	2124.2281	47 075.923	0.073	0.020	$(^2F)4s\,^3F_4$ – $(^2F)4p\,^3G_5$	
3.68	0.459	4	2122.4806	2123.1516	47 099.792	−0.178	0.057	$(a^2D)4s\,^3D_2$ – $(a^2D)4p\,^3D_2$	III
3.68	0.459	4	2122.4806	2123.1516	47 099.792	−0.288	0.057	$(a^2D)4s\,^3D_3$ – $(a^2D)4p\,^3D_2$	III
2.97	0.106	3	2119.6372	2120.3077	47 162.967	0.037	0.018	$(^2H)4s\,^3H_5$ – $(^2H)4p\,^1G_4$	
3.74	0.337	4	2118.6949	2119.3652	47 183.941	0.121	0.042	$(a^2D)4s\,^3D_1$ – $(a^2D)4p\,^3D_1$	
3.63	0.212	6	2117.9054	2118.5755	47 201.528	−0.002	0.018	$(^4F)4s\,^5F_1$ – $(^4F)4p\,^5D_0$	II

Table 1 – *continued*

Integrated intensity[a]	FWHM[b] (cm^{-1})	SNR[c]	λ_{air} (Å)	λ_{vac} (Å)	σ (cm^{-1})	Differences[d] (cm^{-1})	Uncertainty[e] (cm^{-1})	Transition Lower	–	Upper	Note[f]
4.88	0.324	84	2117.5519	2118.2219	47 209.407	−0.024	0.003	$(^4F)4s\,^5F_5$	–	$(^4F)4p\,^5F_5$	
4.72	0.327	55	2114.8948	2115.5643	47 268.713	−0.027	0.006	$(^4F)4s\,^5F_4$	–	$(^4F)4p\,^5F_4$	G
3.95	0.395	8	2114.5634	2115.2328	47 276.120	0.060	0.025	$(a^2D)4s\,^3D_2$	–	$(a^2D)4p\,^3D_3$	III
3.95	0.395	8	2114.5634	2115.2328	47 276.120	−0.050	0.025	$(a^2D)4s\,^3D_3$	–	$(a^2D)4p\,^3D_3$	III
4.18	0.327	15	2114.3032	2114.9726	47 281.936	0.056	0.011	$(^4F)4s\,^5F_1$	–	$(^4F)4p\,^5D_1$	
4.60	0.325	41	2113.8331	2114.5024	47 292.451	0.051	0.004	$(^4F)4s\,^5F_3$	–	$(^4F)4p\,^5F_3$	
4.43	0.331	27	2113.7634	2114.4327	47 294.009	0.029	0.006	$(^4F)4s\,^5F_2$	–	$(^4F)4p\,^5D_2$	
3.42	0.147	5	2107.7207	2108.3888	47 429.583	−0.077	0.015	$(^4F)4s\,^5F_1$	–	$(^4F)4p\,^5D_2$	
3.86	0.278	7	2106.8202	2107.4881	47 449.853	0.003	0.020	$(^4F)4s\,^5F_2$	–	$(^4F)4p\,^3D_1$	
4.30	0.336	15	2105.5878	2106.2555	47 477.621	0.051	0.011	$(^4F)4s\,^5F_3$	–	$(^4F)4p\,^3D_2$	
4.20	0.268	11	2104.8949	2105.5625	47 493.248	0.078	0.012	$(^4F)4s\,^5F_2$	–	$(^4F)4p\,^5F_3$	
4.13	0.317	11	2103.3430	2104.0102	47 528.287	−0.143	0.015	$(^4F)4s\,^5F_4$	–	$(^4F)4p\,^5F_5$	
4.34	0.350	14	2103.2228	2103.8900	47 531.003	0.023	0.013	$(^4F)4s\,^5F_3$	–	$(^4F)4p\,^5F_4$	
3.46	0.151	5	2100.8152	2101.4819	47 585.468	−0.062	0.015	$(^4F)4s\,^5F_1$	–	$(^4F)4p\,^3D_1$	
4.09	0.299	9	2100.4935	2101.1602	47 592.754	−0.026	0.017	$(^4F)4s\,^5F_4$	–	$(^4F)4p\,^3D_3$	
3.54	0.224	2	2078.4070	2079.0694	48 098.443	0.083	0.056	$(a^2D)4s\,^3D_2$	–	$(a^2D)4p\,^3P_2$	III
3.54	0.224	2	2078.4070	2079.0694	48 098.443	−0.027	0.056	$(a^2D)4s\,^3D_3$	–	$(a^2D)4p\,^3P_2$	III
4.66	0.295	7	2055.0703	2055.7219	48 644.711	0.151	0.021	$(a^2D)4s\,^3D_1$	–	$(a^2D)4p\,^3P_0$	

[a]The logarithm (to the base ten) of the integrated intensity (arbitrary units).
[b]FWHM.
[c]The SNR.
[d]Differences ($\sigma_{obs} - \sigma_{Ritz}$) between the FTS observed wavenumbers (σ_{obs}) and the Ritz wavenumbers (σ_{Ritz}) from Ekberg (1997).
[e]The wavenumber uncertainty of the line.
[f]Note provides additional information about the line, as follows:
II: blended or doubly identified with a Cr II line;
III: blended or doubly identified with a Cr III line;
G: a COG line fit (otherwise least-squares fit to Voigt profile).

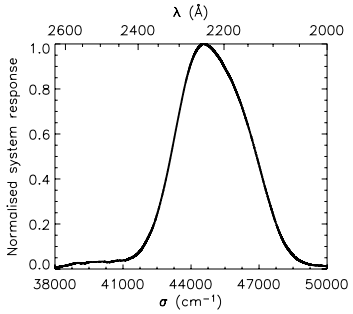

Figure 4. Normalized system response for the Cr–Ne PDL FTS measurements.

FWHM, in cm^{-1}, and the SNR are given in the second and third columns, respectively. Air wavelengths, in Å, presented in the fourth column, were calculated from the observed wavenumbers using the formula for the dispersion of air from Edlén (1953). The observed vacuum wavelengths, in Å, and vacuum wavenumbers, in cm^{-1}, are given in the fifth and sixth columns, respectively. Wavenumber differences ($\sigma_{obs} - \sigma_{Ritz}$) between the measured spectral lines (σ_{obs}), and the Ritz wavenumbers (σ_{Ritz}) calculated using the energy levels from Ekberg (1997), are given in the seventh column. Wavenumber uncertainties for the lines, calculated in quadrature from the wavenumber calibration and estimated line-fitting uncertainties, are given in eighth column. The ninth and tenth columns give the designations of the lower and upper energy levels, respectively, involved in the transition. The final column indicates any blends or doubly identified lines and COG fits.

5 THE CLASSIFICATION OF THE CR III SPECTRUM

The classification of the observed Cr III lines was achieved by comparison of the observed spectrum with Ritz wavelengths generated using the energy levels from Ekberg (1997). A neon linelist comprising Ne II and Ne III lines from the NIST Atomic Spectra Data base (ASD; http://physics.nist.gov/asd3) was used to identify lines from the buffer gas. Cr I and Cr II energy levels, also from the NIST ASD, were used to identify the transitions involving the lower ionization stages of Cr. In total, 140 $3d^34s - 3d^34p$ transition lines were classified as Cr III in the range 38 207 to 48 645 cm^{-1}; 26 of these lines are identified as blends (or doubly identified) with Cr II or other Cr III lines. The $(^4F)4s\,^5F_4 - (^4F)4p\,^5G_4$ transition at 44 284.843 cm^{-1} was not observed in Ekberg (1997), although it was previously observed in Ekberg (1976). In addition, the line at 45 209.622 cm^{-1}, classified as $(a\,^2D)4s\,^3D_2 - (^4P)4p\,^3D_3$ and $(a^2D)4s\,^3D_3 - (^4P)4p\,^3D_3$ for our FTS measurements and in Ekberg (1976), were mislabelled as $(a^2D)4s\,^3D_2 - (a^2D)4p\,^3F_3$ and $(a^2D)4s\,^3D_3 - (a^2D)4p\,^3F_3$ in Ekberg (1997). Wavenumber differences between the observed FTS unblended lines, σ_{obs}, and the Ritz wavenumbers generated from Ekberg (1997), σ_{Ritz}, are shown in Fig. 5. The error bars represent the FTS line-fit uncertainties.

The mean of $\sigma_{obs} - \sigma_{Ritz}$ is small, $\approx$0.002 cm^{-1}, with a scatter about this value having a standard deviation of 0.1 cm^{-1}. This indicates there is no significant systematic error in wavenumber between the two sets of measurements. The estimated uncertainty in the observed wavelengths of Ekberg (1997) is 5 mÅ, which corresponds to an uncertainty of 0.1 cm^{-1} at 45 000 cm^{-1}, very close to the standard deviation of the differences between the FTS measured wavenumbers and the Ritz wavenumbers. The Ritz wavelengths

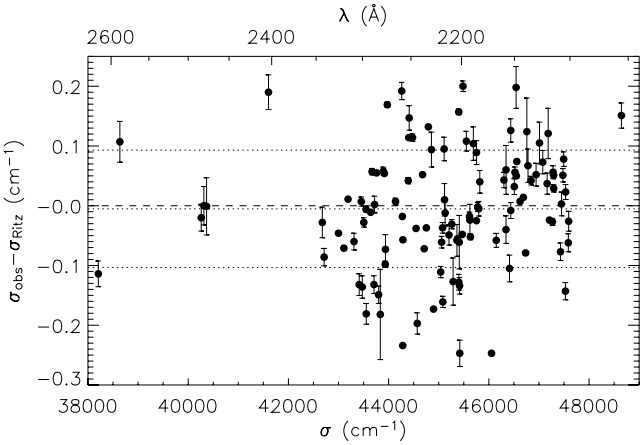

Figure 5. Wavenumber differences between the FTS measured, unblended Cr III lines, σ_{obs}, and the Ritz wavenumbers from Ekberg (1997), σ_{Ritz}. The error bars represent the FTS measured line-fitting uncertainties.

from Ekberg (1997) would be expected to be more accurate than his observed wavelengths, since Ritz wavelengths are generated from the energy levels that were fitted using all classified observed lines, and therefore their uncertainty should not exceed 5 mÅ, in general. The energy level uncertainties given in Ekberg (1997) vary for the $3d^3 4s$ and $3d^3 4p$ levels, with most in the range 0.05 to 0.1 cm^{-1}. Combining the uncertainty of two levels in quadrature gives the estimated uncertainty of the Ritz wavenumbers as approximately 0.1 cm^{-1}, as expected.

An example of the higher resolution and greater accuracy obtainable with FTS spectra, compared with the previous grating spectra, can be seen in Fig. 6. The two lines shown, $(^4F)4s\ ^5F_3 - (^4F)4p\ ^5F_3$ and $(^4F)4s\ ^5F_2 - (^4F)4p\ ^5D_2$, were labelled as a single-blended broad line in Ekberg (1997), and were thus given the same wavelength and intensity parameters. The FTS measured lines are fully resolved.

6 ENERGY LEVEL ANALYSIS

With sufficient, accurate, observed transition lines, known energy levels can be improved through a weighted least-squares fitting process. Preliminary reworking of a small number of $3d^3(^4F)4s$ and $3d^3(^4F)4p$ energy levels, using the ELCALC program (Radziemski & Kaufman 1969), with the weightings of the observed lines inversely proportional to the square of the wavenumber uncertainties, showed that order of magnitude improvements in the energy level accuracies were possible for some of the levels. However, due to the relatively small number of lines, a full reworking of the energy levels was not attempted and is not included here. There are few or no observed interparent transition lines in many cases, which would make it difficult to place all of the energy levels on the same relative scale. The classified lines, however, are of significance in their use as wavelength standards for analysis of stellar spectra, with several of the Cr III transitions having already been observed in recently acquired B star spectra (Peters, private commumication).

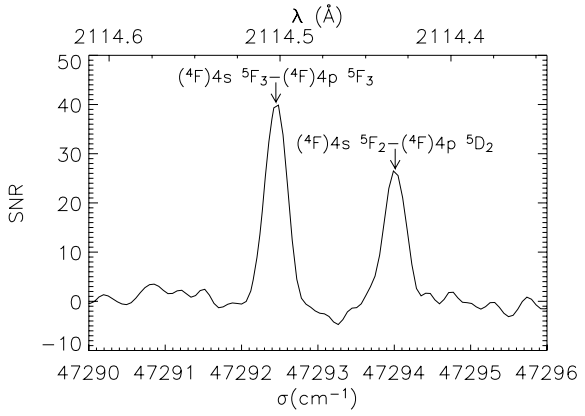

Figure 6. The spectral lines $(^4F)4s\ ^5F_3 - (^4F)4p\ ^5F_3$ and $(^4F)4s\ ^5F_2 - (^4F)4p\ ^5D_2$ were observed as a single broad-line feature in the grating spectrum of Ekberg (1997) and are fully resolved in the FTS Cr III spectrum, as shown.

7 SUMMARY

Previous measurements of doubly ionized spectra of the iron group elements, vital for analysis of hot B stars, have used grating spectrographs with typical wavelength uncertainties of 5 mÅ (a few parts in 10^6). The high-resolution modern astrophysical spectrographs have increased both the wavelength coverage and resolution of stellar spectra, with wavelength uncertainties of one part in 10^7 in the UV required for their full interpretation. This work represents the first measurements of the Cr III spectrum by FTS, using a Cr–Ne PDL. 140 $3d^3 4s$–$3d^3 4p$ Cr III transition lines in the region 38 000 to 49 000 cm^{-1} are presented. The wavenumber uncertainties of the strongest lines approach 0.002 cm^{-1} (0.1 mÅ at 2200 Å), a reduction in uncertainty by a factor of 50 over the observed grating lines measured by Ekberg (1997).

ACKNOWLEDGMENTS

DGS gratefully acknowledges technical advice from R. J. Blackwell-Whitehead. This work was funded by NASA Grant NAG5-12668, The Leverhulme Trust and PPARC of the UK.

REFERENCES

Cowley C., Frey M., 1988, Nucl. Instrum. Methods B, 31, 214
Davis S., Abrams M., Brault J., 2001, Fourier Transform Spectrometry. Academic Press, New York
Edlén B., 1953, J. Opt. Soc. Am., 43, 339
Ekberg J., 1976, Phys. Scr., 14, 109
Ekberg J., 1997, Phys. Scr., 56, 141
Finley D., Bowyer S., Paresce F., Maline R., 1979, Appl. Opt., 18, 649
Heise C., Hollandt J., Kling R., Kock M., Kühne M., 1994, Appl. Opt., 53, 5111
Johansson S., 1987, Phys. Scr., 36, 99
Kurucz R., 2002, in Schultz D., Krstic P. S., Own by F., eds, Proc. AIP Conf., Vol. 636, Am. Inst. Phys., New York, p. 134
Learner R. C. M., Thorne A. P., 1988, J. Opt. Soc. Am. B, 5, 2045
Leckrone D., Johansson S., Wahlgren G., Proffitt C., Brage T., 1996, Phys. Scr. T, 65, 110
Murray J. E., 1992, PhD thesis, Univ. of London
Nave G., Johansson S., Learner R., Thorne A. P., Brault J., 1994, ApJS, 94, 221
Nave G., Sansonetti C., Griesmann U., 1997, Opt. Soc. Am. Tech. Dig., Vol. 3, Fourier transform spectroscopy, Opt. Soc. Am., Washington D.C., p. 38
Pickering J. C., 2002, Vib. Spectrosc., 29, 27
Pickering J. C., Thorne A. P., 1996, ApJS, 107, 761
Pickering J. C., Raassen A., Uylings P., Johansson S., 1998, ApJS, 117, 261
Radziemski L., Jr, Kaufman V., 1969, J. Opt. Soc. Am., 59, 424
Ralchenko Y., Jou F.-C., Kelleher D. et al., 2007, NIST Atomic Spectra Data base (version 3), (http://physics. nist.gov/asd3)
Smillie D. G., 2007, PhD thesis, Univ. of London

Smillie D. G., Pickering J. C., Smith P. L., Nave G., Blackwell-Whitehead R., 2006, in Weck P., Kwong V., Salama F., eds, Proc. 2006 NASA Laboratory Astrophysics Workshop (NASA/CP-2006-214549), NASA Ames, Moffett Field, p. 256

Smith P. L., Thorne A. P., Learner R. C. M., Pickering J. C., Kling R., Mende W., Kock M., 1998, in Brandt J. C., Ake T. B., Petersen C. C. Scientific impact of the Goddard High Resolution Spectrograph. ASP Conf. Ser. Vol. 143. Astron. Soc. Pac., San Francisco, p. 395

Swings J., Klutz M., Vreux J., 1976, A&AS, 25, 193

Thorne A. P., 1996, Phys. Scr. T, 65, 31

Whaling W., Anderson W., Carle M., Brault J., Zarem H., 1995, J. Quant. Spectrosc. Radiat. Transfer, 53, 1

This paper has been typeset from a TEX/LATEX file prepared by the author.